# Van der Waals materials integrated nanophotonic devices [Invited]

CHANG-HUA LIU,[1,*] JIAJIU ZHENG,[2] YUEYANG CHEN,[2] TAYLOR FRYETT,[2] AND ARKA MAJUMDAR[2,3,*]

[1]*Institute of Photonics Technologies, National Tsing Hua University, Hsinchu 30013, Taiwan*
[2]*Department of Electrical and Computer Engineering, University of Washington, Seattle, WA 98195, USA*
[3]*Department of Physics, University of Washington, Seattle, WA 98195, USA*
[4]*chliu@ee.nthu.edu.tw*
[5]*arka@uw.edu*

**Abstract:** Emerging van der Waals materials exhibit a wide range of optical and electronic properties, making them attractive for nanophotonic devices. Due to the nature of van der Waals interactions, this new class of materials can be readily integrated with other existing nanophotonic structures, leading to novel device architectures and operating principles. In this review, we will present the progress of active nanophotonics, realized by integrating van der Waals materials with on-chip optical waveguides or resonators. Additionally, we will review the emerging research area in van der Waals nanophotonics, where the nanophotonic structures are fully made of van der Waals materials. A variety of van der Waals nanophotonic structures, ranging from ultrathin Fresnel lens, metasurfaces to photonic crystal cavities and their potential impacts on miniaturized optical system and quantum technology will be discussed.

## 1. Introduction

Integrated nanophotonics hold the key for ultimate miniaturization of optical devices, while simultaneously achieving energy-efficiency and high speed operation [1], with far-reaching impact on the next-generation optical information processing, communication and sensing systems. Several recent works demonstrated an unprecedented level of integration of photonic devices, primarily enabled by semiconductor nanofabrication [2,3]. Going beyond traditional applications involving optical transceivers for data-communication [4], the photonic integrated circuits are finding applications in optical information processing [5], quantum simulation [6], linear optical quantum computing [7], and optical phased array [7,8]. While novel device design and fabrication are necessary to advance this research field, a crucial component is new material systems to realize active devices, including light sources, modulator, detectors and nonlinear optical structures. In this regard, low-dimensional materials, such as quantum confined structures hold great promise, primarily due to the enhanced density of states, leading to energy efficient and compact devices.

One such low-dimensional material is atomically thick layered van der Waals (vdW) materials. This new class of material are alluring for optoelectronics applications, as they have a wide range of optical band gap and electrical transport properties [9–11]. For example, graphene is a semi-metal with zero band gap, while transition metal dichalcogenides (TMDCs) and black phosphorous (BP) are semiconductors with band gap covering the technologically important visible and infrared wavelength regimes. Hexagonal boron nitride (hBN) is an atomically-thin insulator with excellent thermal stability and chemical inertness. Beyond usual optoelectronic properties, several newly discovered vdW materials show correlated characteristics in the two-dimensional (2D) limit, such as superconductivity, ferroelectricity and ferromagnetism [11–14]. These unconventional material properties could

potentially increase the functionalities of devices at the nanoscale. And most importantly, due to the nature of vdW interactions, the layered materials can be integrated onto different substrates, which makes them a promising candidate for integrated photonics applications [15,16].

In this paper, we review the current status of various active devices, including light emitters, modulators, photodetectors and nonlinear optical structures, enabled by vdW or 2D (i.e. vdW material in the single-layer limit) materials integrated with nanophotonic structures, such as waveguides or nano-resonators. We then highlight the new opportunities of integrated nanophotonics, created by patterning vdW materials themselves into nanostructures. The future directions and challenges of vdW photonics are also discussed.

## 2. Light emitters integrated with nanophotonics

On-chip light emitters are crucial components for any integrated photonic system. vdW materials with direct band gap in the monolayer limit are extremely attractive for creating such light sources. Unlike the wafer-bonding of III-V material on silicon, vdW materials can be easily integrated with the underlying large-scale photonic integrated circuit, fabricated via CMOS-compatible manufacturing. Photoluminescence (PL) from TMDCs have shown their band gaps are from the near-infrared to the visible spectral region (1-2.5 eV) [9,10]. BP has also garnered significant attention, as its band gap and electronic structure are layer-dependent, with band gaps spanning from 0.3 eV in bulk to 2 eV in monolayer [10]. More strikingly, when the thickness of these vdW materials approach the atomic limit, weak dielectric screening from the environment has been predicted to cause strong Coulomb interactions of photoexcited electron-hole pairs and thus, form strongly bound excitons (~hundreds of meV) [17]. Such a phenomenon has yet to be observed in bulk semiconductors but is particularly beneficial for developing light emitting devices. Despite these promising characteristics, the emitted power of ultrathin materials is too low for practical applications. Using nanophotonic resonators, however, we can enhance the light emission due to temporal and spatial confinement of light.

### 2.1 Enhanced light-matter interactions

Optical cavities can trap photons for substantial period of time and manipulate the electromagnetic environment (i.e. the local optical density of states). Thus, they can significantly modify the emission and absorption characteristics of materials. The efficacy of 2D material integrated devices was in part demonstrated by Wu et al., who transferred a monolayer tungsten diselenide (WSe$_2$) onto a linear three-hole (L3) defect gallium phosphide photonic crystal cavity (PhCC) [Fig. 1(a)] [18]. The resonance wavelength of PhCC overlaps with the PL spectrum of WSe$_2$, and the cavity quality factor is ~180. The PL collected from the cavity region shows a prominent cavity-enhanced peak, with an intensity ~60 times stronger than the off photonic crystal region [Fig. 1(b)]. Additionally, the cavity-enhanced PL is linearly polarized and aligned with the polarization of the corresponding cavity mode [Fig. 1(c)]. A similar experiment was reported with MoS$_2$ [19], and cavity-enhanced PL was also observed by several research groups by integrating 2D onto different linear line defect PhCC, distributed Bragg reflector (DBR), microdisk optical resonators [19–21] and 1D photonic crystal cavities made of silicon nitride [22] and silicon dioxide [23]. We note that, however, the Purcell enhancement of TMDCs depends only on the cavity mode-volume and not quality factor, as the TMDC exciton-cavity operates at the good cavity regime (i.e. emitter linewidth larger than the cavity linewidth) [24,25]. Broad emitters coupled with large non-radiative decay of the TMDCs exciton further makes accurate measurement of the Purcell enhancement difficult.

While most of the research on cavity enhanced light emission from vdW materials focus on weak coupling regime, few works involving DBR resonators demonstrated strong coupling of the cavity mode and 2D exciton. The resulting exciton-polariton systems are probed by

either energy-momentum spectroscopy, or by tuning the cavity length to demonstrate anti-crossing at room temperature [26–28]. Very recently, the directional excitation of polaritons has also been realized based on the graphene-hexagonal boron nitride heterostructures [29,30].

## 2.2 Optically-pumped nanolasers

Although the early experiments successfully demonstrated cavity-enhanced PL, the lasing behaviors were not observed from these hybrid systems owing to the low Q-factor of the cavities. One route to realize nanolasers based on the atomically-thin gain medium is to further improve the cavity Q-factor to compensate the limited material gain volume. For instance, the Q-factor of GaP PhCC can be increased to ~2500 after the monolayer $WSe_2$ transfer by optimizing its thickness-to-lattice-constant ratio and sidewall verticality [31] [Fig. 1(d-e)]. Additionally, creating $Si_3N_4$/monolayer $WS_2$/hydrogen silsesquioxane (HSQ) microdisk structure could offer strong optical confinement and lead to whispering gallery resonance with Q-factor ~2604 [32] [Fig. 1(f)]. These two hybrid systems have large modal gain, and thereby, exhibit the signatures of lasing at low-threshold optical pumping power under cryogenic temperature. Later papers reported room temperature lasing in the visible regime via implementing multilayer $MoS_2$ onto a microdisk resonator (Q: 2600-3300) [Fig. 1(g)] [33]. More recently, lasing in the infrared regime ($\lambda$~1132 nm) at room temperature was also demonstrated by coupling $MoTe_2$ to a silicon nanobeam cavity (Q~5603) [34], as shown in Fig. 1(h). While in all these works, clear nonlinear input-output behavior was observed, which was attributed to optically pumped laser, more conclusive proof of lasing, including of second-order autocorrelation was not reported, and remains to be measured.
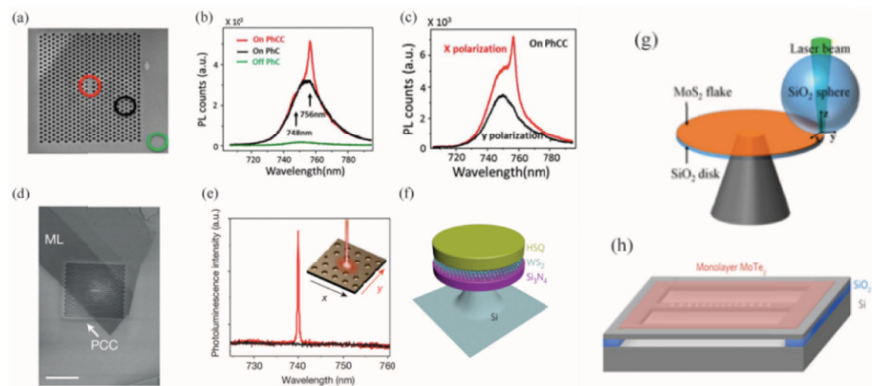


Fig. 1. Cavity-enhanced PL of 2D materials. (a) Scanning electron micrograph (SEM) of the hybrid monolayer $WSe_2$-PhC nanostructure. (b) Spatial-dependent PL measured from the device shown in (a). (c) Polarization-dependent PL measured from the PhCC area shown in (a). (d-e) Integration of monolayer $WSe_2$ with a high-Q PhCC, and its (d) SEM image, and (e) polarization-dependent PL. The results suggest lasing behavior. (f-h) Other optically-pumped lasers based on (f) Monolayer $WS_2$ laser coupled with a HSQ/ $Si_3N_4$ disk resonator, (g) $MoS_2$ flake coupled with a $SiO_2$ disk resonator, and (h) Monolayer $MoTe_2$ coupled with a Si nanobeam. Figures are adapted with permission from: (a-c) [18], Institute of Physics Publishing; (d-e) [31], Nature Publishing Group; (f) [32], American Chemical Society; (g) [33], American Chemical Society; (h) [34], Nature Publishing Group.

## 2.3 Electrically-pumped light emitters integrated with the cavity

All the works presented so far involves optical pumping. For practical application, however, we need electrically pumped cavity-enhanced light sources. A wide range of device concepts and architectures have been demonstrated for 2D material based light emitting diodes (LED). The earlier works exploited the recombination of electron-hole pairs from the in-plane 2D-metal Schottky junctions or p-n junctions to realize atomically-thin LEDs [35–38]. But the

external quantum efficiency is only ~1%, and the light emitting area is limited to within the junction area (typically less than 1 μm). Withers et al. utilized the dry transfer technique to create a vdW tunneling diode, consisting of a monolayer TMDCs sandwiched between two tunneling contacts formed by graphene and hexagonal boron nitride [39]. Built on this design, the LED can exhibit higher quantum efficiency (~10%) and electroluminescence (EL) can occur from the whole TMDCs area. To enhance the efficiency, Liu et al. further proposed a novel device concept by integrating a gallium phosphide PhCC (Q~100) on top of a vdW LED [40], as shown in Fig. 2(a). The device demonstrated cavity-enhanced (>4 times, Fig. 2(b)) and highly linear polarized (84%) EL at room temperature, with a direct modulation speed of ~1 MHz [Fig. 2(c)]. This reported speed is faster than the most in-plane optoelectronics based on TMDCs, as the current injections of those in-plane devices are usually limited by TMDCs/metal Schottky barriers. More importantly, the observation of cavity-enhanced EL suggests the possibility to realize an electrically-pumped laser in this platform.
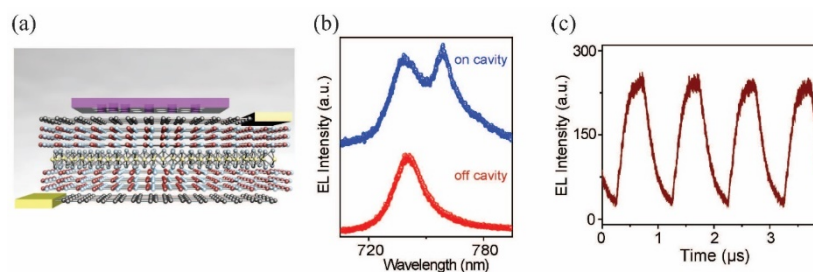


Fig. 2. Cavity-integrated vdW light emitting diode. (a) Schematic of the device structure. (b) Electroluminescence signal measured from on-cavity and off-cavity areas. (c) Modulation of electroluminescence at 1 MHz speed. Figures are adapted with permission from [40], American Chemical Society.

## 3. Modulator

As one of the most crucial technologies in nanophotonics, optical modulation has been extensively studied aiming for high-performance optical interconnects, sensing, information processing, and beam steering [41]. vdW materials have been used to create broadband, compact, energy-efficient, and ultrafast optical modulators, and their extreme thinness can potentially enable ultra-low energy operation.

### 3.1 Electro-optic modulators

Electro-optic modulation is the most investigated technology in current vdW material-based optical modulators targeting high-speed applications. These devices primarily utilize the gate-tunable electro-absorption or electro-refractive effect in graphene. Liu et al. was the first to demonstrate a broadband (1.35 μm to 1.6 μm), high-speed (1 GHz), and compact (25 μm$^2$) waveguide-integrated electro-absorption modulator based on monolayer graphene [Fig. 3(a)] [42]. By electrically tuning the Fermi level of the graphene sheet in a carrier-accumulation capacitor structure [Fig. 3(b)], the transmission of the device was modulated by 0.1 dB/μm due to Pauli blocking effect [Fig. 3(c)]. Built on this foundation, the double-layer graphene structure was proposed, which can provide better modulation depth (0.16 dB/μm) [43], with an insertion loss ~0.9 dB [44]. Additionally, the double-layer graphene optical modulators can avoid the slow carrier transport in silicon [42,45], allowing for operation speeds approaching 35 GHz [44].

Whereas the increased modulation helps reduce the footprint and energy consumption, further improvement of these figures of merit requires stronger light-matter interaction. One effective solution is to conduct optical modulation by integrating vdW materials with optical cavities, such as PhCC [46,47], microring resonators [48,49], or nanobeam cavities [50]. Gao

et al. reported a graphene–hBN heterostructure-based electro-optic modulator coupled with a silicon PhCC [Fig. 3(d)], and its active area is only ~0.5 μm$^2$ [51]. Similarly, Phare et al. utilized a silicon nitride microring resonator [Fig. 3(e)] and demonstrated a 30 GHz graphene electro-optic modulator based on the critical coupling effect. The achieved modulation efficiency was 1.5 dB/V with an energy consumption of just 800 fJ/bit [52].

Despite many advantages, resonant-structure-based modulators suffer from high sensitivity to temperature variations, fabrication tolerances [41] and narrow optical bandwidth. To address these, one alternative approach is to use slot waveguides or plasmonic waveguides. In the latter case, either waveguides based on graphene surface plasmon polariton (SPP) or SPP waveguides from other materials are exploited [53–55]. Ansell et al. fabricated a proof-of-concept hybrid graphene plasmonic waveguide modulator based on the graphene/hBN/metal structure with an active area of just 10 μm$^2$ operating at telecom wavelengths [56]. With the aid of low-loss metal plasmonic slot waveguides, Ding et al. reported a graphene electro-absorption modulator showing a modulation depth of 0.13 dB/μm [57]. By inserting graphene into a hybrid metal-oxide-silicon (MOS) plasmonic waveguide, a compact (~10 μm) electro-absorption modulator with a modulation depth >0.2 dB/μm and energy consumption of only 110 aJ/bit is recently reported [58], confirming the theoretical limits of switching energy is below 1 fJ/bit [59].
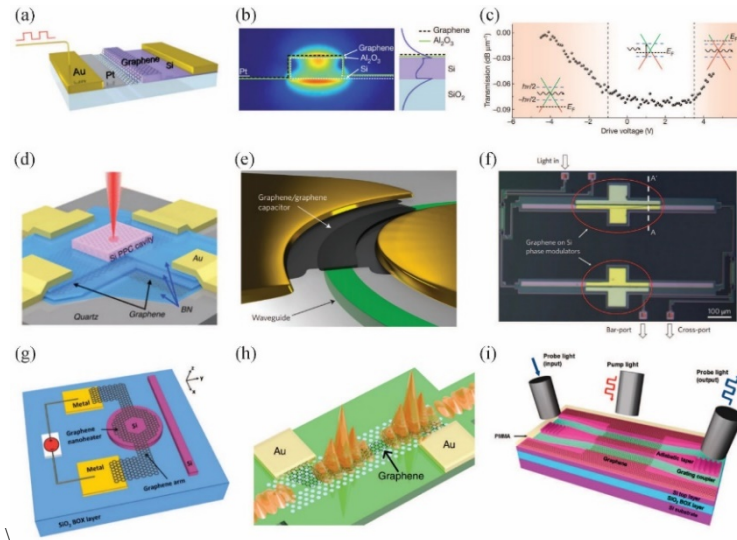


Fig. 3. Optical modulators based on vdW-integrated nanophotonic structures. (a) Schematic of the first graphene-integrated waveguide-based modulator, its (b) cross sections with an overlay of the mode profile, and the (c) static electro-optical response at different drive voltages. (d) Schematic of a graphene–hBN heterostructure-integrated silicon PhCC modulator. (e) Schematic of a graphene- silicon nitride microring modulator. (f) Optical image of the MZI-based graphene-silicon phase modulators. (g) Schematic of a thermally tunable silicon micro-disk with a transparent graphene nano-heater. (h) Schematic of a slow-light-enhanced graphene heater. (i) Schematic of a graphene-silicon hybrid all-optical modulator. Figures are adapted with permission from: (a-c) [42], Nature Publishing Group; (d) [51], American Chemical Society; (e) [52], Nature Publishing Group; (f) [60], Nature Publishing Group; (g) [66], Optical Society of America; (h) [67]; (i) American Chemical Society.

Another way to realize optical modulators is to exploit the electro-refractive effect. In 2017, Sorianello et al. reported a graphene-silicon phase modulator by exploiting the Mach–Zehnder interferometer (MZI) configuration [Fig. 3(f)] [60]. The compact (300 μm) device exhibits an enhanced modulation efficiency of 0.28 V·cm (outperforming the state-of-the-art silicon depletion-mode modulators [61]), a high extinction ratio of 35 dB, and suppressed optical loss when operated in the Pauli blocking regime. The device had an electro-optical

bandwidth of 5 GHz and operated at 10 Gb/s with 2 V peak-to-peak driving voltage in a push-pull configuration.

## 3.2 Thermo-optic modulators

Thermo-optic modulation relies on the change of material refractive index induced by temperature. This kind of modulator has long time constant, limiting device operation speed to anywhere between the kilohertz to megahertz range. Graphene is considered as an attractive material for energy-efficient, and compact, and cost-effective thermal management due to its high intrinsic thermal conductivity, electric conduction, transparency, and ease of fabrication. Specifically, graphene has been used as an efficient heat conductor, electrical heater, and optical heater for thermo-optic modulation primarily in silicon photonics. As a transparent flexible conductor, graphene has been used for efficient thermal tuning of a silicon MZI and micro-disk resonator [62]. Other integrated nanophotonic structures, including graphene plasmonic waveguides [63], microrings [64,65], microdisks [Fig. 3(g)] [66], slow-light photonic crystal waveguides [Fig. 3(h)] [67], and nanobeam cavities [68,69] have been introduced to reduce the power consumption by increasing either the group index or the quality factor. Use of resonators also increases the thermal and optical confinement and reduce the thermal time constant. As a result, graphene-based thermo-optic modulators have exhibited a high modulation depth up to 30 dB [63], a 10%-90% rise time of 750 ns [64,67], a large energy efficiency from 1.67 nm/mW [66] to 10 nm/mW [68], a low switching power of 0.11 mW [68], and a figure of merit (defined as the inverse of the product of rise time and power consumption) as large as 0.67 $nW^{-1}s^{-1}$ [67], comparable or even better than the traditional silicon photonic thermo-optic modulators [70]. Due to this high performance, graphene-based thermo-optic modulators have recently been proposed to improve optical phased arrays (OPAs) essential for light detection and ranging (LIDAR) systems [71].

## 3.3 All-optical modulators

The growing research in optical interconnects may ultimately need all-optical modulation to circumvent the excess energy consumption and latency during the electro-optic signal conversion [72]. The majority of all-optical modulators using vdW materials are based on saturable absorption for absorptive modulation and optical Kerr effect for refractive modulation. Recent theoretical analysis proved that for graphene-on-silicon all-optical modulators, absorptive modulation mode is more suitable with a required optical pump intensity of 10MW/$cm^2$ and a short length of ~200 μm, much better than those based on refractive modulation and far better than those based on bare silicon waveguides [73]. With the aid of saturable absorption and photoluminescence of $WS_2$, Yang et al. modulated and amplified an optical signal at 640 nm with a 532 nm pump on a silicon nitride waveguide [74]. Another way to perform all-optical modulation is via photogating effect. Yu et al. demonstrated such all-optical modulation on graphene-silicon hybrid waveguides [Fig. 3(i)] [75]. By pumping the device with an ultra-low visible light power of 0.1 mW (corresponding to 2 W/$cm^2$ in intensity, seven orders of magnitude lower than that for saturable absorption), carriers are generated in silicon. Assisted by the built-in electric field in the graphene-silicon junction, the Fermi level of p-type graphene is lowered, resulting in suppressed graphene absorption over a broadband (>80 nm) infrared probe light. Thanks to the ultra-long diffusion length of the carriers originated from the large mobility of graphene, this all-optical modulation can also be nonlocally conducted with a distance between the device and the spot of pump light longer than 4 mm, implying its applications in position sensing and remote controlling [76].

## 4. Photodetectors

The discovery of graphene generated an intense research effort on understanding its photoresponse, as graphene has exceptional high carrier mobility, strong light absorption

coefficient and unique quantum confinement effects arising from its atomic thickness. Thus far, different mechanism of photoresponses were reported, including photo-voltaic, -gating, -thermoelectric, -Dember, -conductivity and bolometric effects [77–84]. Understanding the underlying mechanisms provided the foundation for developing graphene and other 2D photodetectors. The unique photoresponse and photodetection applications of 2D materials can be found in other review articles [85,86]. Here, we focus on reviewing the state-of-the-art photodetectors based on graphene, TMDCs and black phosphorous, integrated with waveguides or optical resonators. Such nanophotonics structures cannot only significantly improve optical absorption of 2D materials, leading more sensitive photodetections, but can also be appealing for integrated nanophotonics applications.

### 4.1 Cavity-Integrated photodetectors

Photodetection based on graphene was generally realized by exploiting photoconductivity or graphene-metal Schottky junctions to separate the photoexcited carriers of graphene [85,86]. Unfortunately, the small area of effective junction region together with limited optical absorption lead to weak responsivity (~mA/W). One approach to address this challenge is to couple optical resonators with graphene photodetectors. Furchi et al. and Engel et al. embedded a graphene layer into a Fabry–Perot micro-cavity [Fig. 4(a)], composed of two Bragg or two metallic mirrors [87,88]. For both experiments, the responsivity of graphene detector is increased by more than 20 times in the visible regime at the cavity resonance wavelength. Another approach is to couple graphene to the evanescent wave of PhCC to increase light-matter interactions. This kind of device has planar, compact structure, and more importantly, it can be easily integrated with on-chip optical interconnects. The cavity-enhanced light absorption in the telecom band was first reported in ref [89]. by integrating graphene onto a Si PhCC as shown in Fig. 4(b). The resulting photocurrent generation is 8-fold enhanced at resonance wavelengths [90] compared to the bare detector. In principle, higher absorption could be realized by further optimizing the Q-factor of resonator, but this would sacrifice the bandwidth of light-matter interaction and the operation speed of detector.
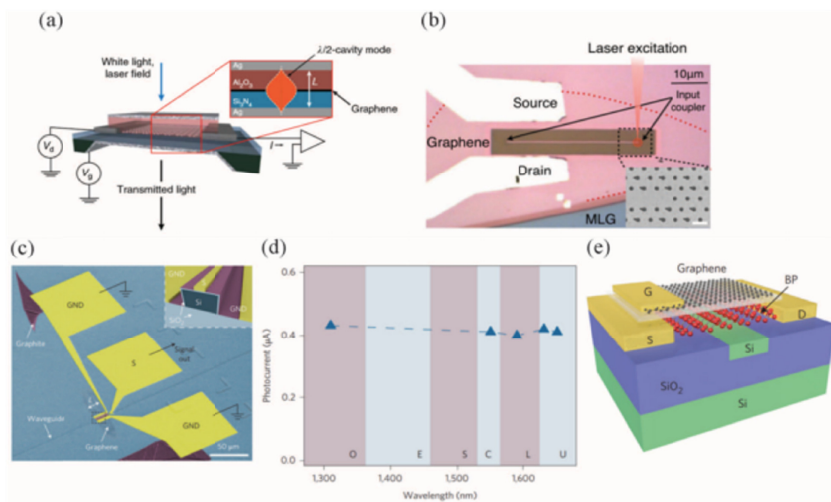


Fig. 4. Photodetectors based on vdW-integrated nanophotonic structures. (a-b) Integrating a graphene photodetector with (a) a microcavity and (b) a PhCC to increase the photoresponsivity. (c) SEM of a Si waveguide-integrated graphene photodetector. (d) Broadband photoresponse of the device shown in (c). (e) Schematic of a Si waveguide-integrated BP photodetector, which has the lower dark current compared with graphene-integrated detectors. Figures are adapted with permission from: (a) [88], Nature Publishing Group; (b) [90], American Institute of Physics; (c-d) [92], Nature Publishing Group; (e) [99], Nature Publishing Group.

## 4.2 Waveguide-Integrated photodetectors

Instead of an optical resonator, high responsivity detectors can also be realized by evanescent coupling to an optical waveguide. Integration with waveguides provides high responsivity (tens to hundreds mA/W), high speed (~20 GHz) and relative broad spectral operation, covering all fiber-optic telecommunication bands [Figs. 4(c) and 4(d)] [91–93]. Based on the progress, the continued effort further optimized the device geometry and improve the RC time constant to enhance the operation bandwidth: different groups have reported ultrafast operation speed, ranging from 40 to 180 GHz [94–98]. More strikingly, those ultrafast integrated photodetectors can be realized by using graphene, grown by chemical vapor deposition (CVD), opening the door for the wafer scale device fabrications and integrations.

In addition to graphene, a waveguide-integrated multilayer BP photodetector was reported recently. The initial study indicates this integrated device could exhibit high responsivity (~hundreds mA/W) and 3 GHz operation speed in an ambient atmosphere condition [Fig. 4(e)] [99]. Importantly, due to the presence of a band gap in BP, the dark current of BP detectors can be more than three orders of magnitude lower than other graphene-based photodetectors. Such feature also suppresses the background noise level, enabling more sensitive measurements.

## 4.3 Other light trapping effects for large area photodetections

For many practical optoelectronics applications, it is desirable to create photonic structures that can enhance the absorption of large-area photoactive layers. To this end, Jariwala et al. exploit the features of high refractive indices and absorption coefficients of TMDCs and demonstrated that near unity absorption could be realized by placing an ultrathin (<15 nm) TMDCs on the reflective metal due to the thin film interference effect (i.e. strongly damped optical modes of TMDCs/metal heterostructures) [100,101]. Other research groups also showed that large area light trapping can be achieved by directly attaching the 2D or vdW materials onto the substrate with prepatterned Fano-resonant structures or a plasmonic antenna array [102–104]. Critically, by exploiting these structures, it is possible to create an atomically-thin and large-area photovoltaic device with its internal quantum efficiency higher than 70% or photodetector with a photo-gain higher than $10^5$ [103,105].

## 5. Nonlinear optics

2D materials, particularly TMDCs, recently emerged as a promising material for nonlinear optics. In particular, due to the lack of centro-symmetry and large excitonic binding energy in the single layer limit, the monolayer TMDCs possess large $\chi^{(2)}$ values [106]. But with an even number of layers, this nonlinearity disappears as the material becomes centrosymmetric. Here, we point out several prominent results in 2D materials integrated nonlinear nanophotonics. A more detailed discussion on this topic can be found out in a recent review [107].

Majumdar et al. theoretically analyzed the layered material clad nano-cavity system and to find the effective nonlinearity [108]. Several groups experimentally demonstrated second harmonic generation (SHG) enhanced by nanophotonic structures, including DBR, PhCC, and waveguides. Day. et al. demonstrated SHG using a 2D $MoS_2$ integrated inside a DBR cavity under pulsed excitation at 800 nm [109], where the DBR is formed by using alternating layers of silicon nitride and silicon dioxide to minimize the light absorption [Fig. 5(a)]. The reported enhancement is around 10. The lower enhancement factor can be attributed to low Q-factor of ~20, and the large mode-volume of the DBR cavity. Using a 2D $WSe_2$ clad silicon PhCC, Fryett et al. demonstrated enhanced SHG. In this work they used a pulsed laser operating within the telecommunication band (~1550 nm) [110]. Figure 5(b) shows the SEM of a 2D $WSe_2$ clad silicon PhCC. When the cavity (resonant at ~1490 nm) is resonantly excited using a pulsed laser, a strong second harmonic signal is observed around 745 nm [Fig. 5(c)]. In the

gaussian background signal from the doubling of the laser by 2D material outside the cavity, they observed a Lorentzian peak at exactly the half-wavelength of the cavity resonance, signifying the cavity-enhanced SHG. The reported enhancement is ~100, primarily because of the lack of a cavity mode at the second harmonic frequency and moderate Q-factor of the cavity (Q ~500). Moreover, silicon absorbs a significant amount of the second harmonic signal. A promising solution will be to make a doubly resonant cavity out of wide bandgap materials, such as silicon nitride or silicon dioxide. Phase-matched SHG was also recently reported in a silicon photonic waveguide using a 2D $MoSe_2$ [Fig. 5(d)] [111]. By engineering the waveguide cross-section, the effective mode-indices of the fundamental and second harmonic modes are matched, which ensures the phase-matching of the light at the fundamental and second harmonic frequencies. Furthermore, the development of double-mode photonic structures is desirable for enhancing the conversion efficiency. Yi et al. demonstrated a double-mode cavity-enhanced SHG from $MoS_2$ using a mechanically tunable Fabry-Perot cavity [112]. The FP cavity comprises of a DBR as the bottom mirror, and the top mirror is a capacitively actuated silver mirror [Fig. 5(e)]. Via mechanical actuation, the fundamental and the second harmonic modes were tuned to the desired frequencies. In this experiment, they used a 2D $MoS_2$ as the nonlinear material, and despite their low cavity Q-factor, the reported enhancement is ~3000. This experiment used a pulsed excitation near 930 nm. Further improvement is possible by improving the cavity Q-factor, and reducing the mode-volume, which is often very large in Fabry-Perot cavities.

The evanescent coupling nature of 2D materials with nanophotonic structures also brings new design principles. Despite increasing fabrication capabilities, it is challenging to precisely fabricate SHG devices with small footprint that are quasi phase-matched. For the conventional device made of the nonlinear material itself, the optical modes are fixed once it is fabricated, and the patterning of the nonlinear material completely changes the confined modes. Fryett et al. theoretically investigated the post-fabrication pattering of TMDCs on ring cavities to reach phase matching [Figs. 5(f) and 5(g)], as the extremely thin 2D material cladding on the cavity would not dramatically affect the modes. The analysis suggests that by patterning 2D materials on a nanocavity with a low inherent nonlinear overlap, we can approach the values of the nonlinear overlap obtained by perfect phase-matching [113].
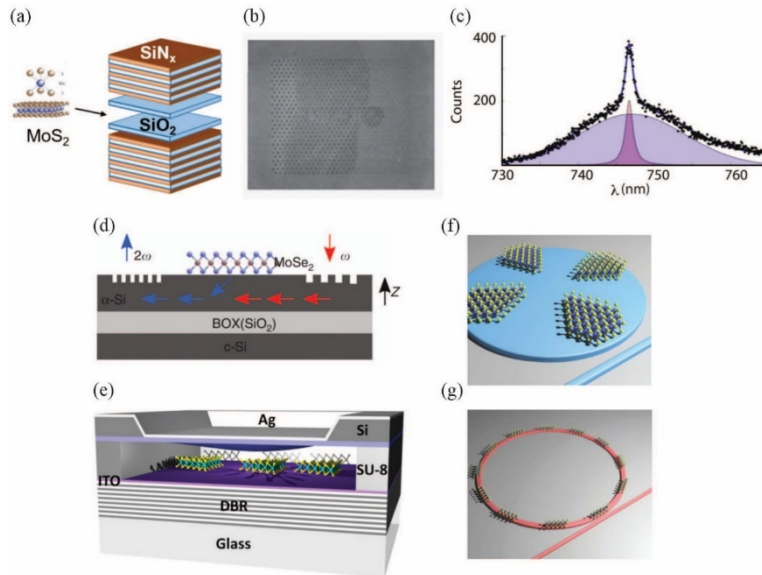


Fig. 5. Cavity-integrated nonlinear optics. (a) DBR cavity enhanced $MoS_2$ SHG. (b) SEM image of the fabricated Si PhCC with monolayer $WSe_2$ on top. (c) The SHG spectrum measured from the device shown in (b). (d) Enhanced SHG of $MoSe_2$ using a Si waveguide.

(e) SHG of $MoS_2$ enhanced by a double mode DBR cavity. (f-g) Phase-matching nonlinear optics via patterning the 2D material. Figures are adapted with permission from: (a) [109], Optical Society of America; (b-c) [110], Institute of Physics Publishing; (d) [111], Nature Publishing Group; (e) [112], American Chemical Society; (f-g) [113], Optical Society of America.

## 6. Van der Waals nanophotonics

In the previous sections, we discussed a wide range of devices via integrating 2D materials or vdW heterostructures with optical resonators or waveguides, which are composed of traditional bulk materials. Distinct from those works, one promising research direction is to directly create the whole nanophotonic structure out of vdW materials. For example, thin Fresnel lenses and gratings have been realized by patterning multilayer high refractive index $MoS_2$ [Fig. 6(a-c)], demonstrating high scattering efficiency [114]. Insulating hBN can support low-loss phonon polaritons, making it ideal for developing mid-infrared hyperbolic metasurfaces [Fig. 6(d)] [115]. Furthermore, hBN intrinsically hosts a high density of defect centers, useful for room temperature single photon source. By fabricating a PhCC from hBN, a unique emitter-cavity hybrid system can be realized with potential applications in quantum information technology [Fig. 6(e)] [116]. Very recently, dielectric metalenses made of vdW materials are demonstrated. Leveraging the incomplete phase design and high indices of vdW materials, the thickness of metalenses can approach $\lambda/10$, while still exhibiting near diffraction-limited focusing and optical imaging [Fig. 6(f-h)]. More intriguingly, due to their vdW nature, the fabricated nanostructured metalenses can be peeled off and then transferred onto different substrates, including flexible substrates, for stretching and tunable focusing applications [117]. We note that, the current development of vdW nanophotonics is still in the early stage, but these recent works have shown the promising future of vdW nanophotonics.
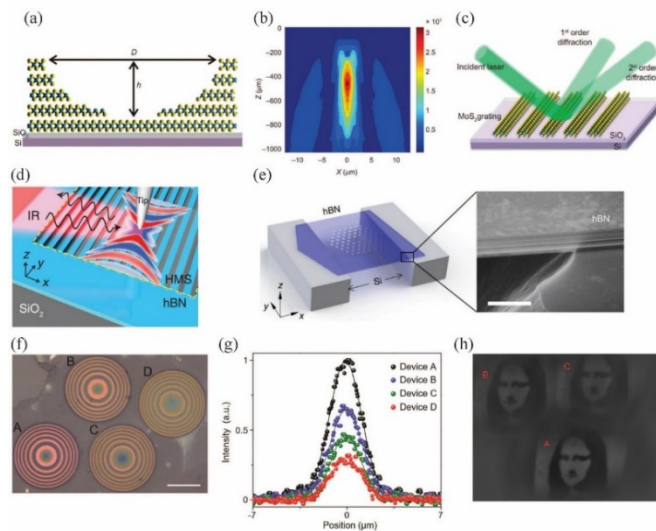
## 7. Outlook and challenges



Fig. 6. Nanophotonics based on vdW materials. (a) The structure of microlens made of a $MoS_2$ flake. (b) Intensity distribution at the focal plane of the $MoS_2$ microlens. (c) Schematic of a nanostructured $MoS_2$ grating. (d) Mid-infrared hyperbolic metasurface made of nanostructured hBN. (e) A suspended PhCC made of hBN. (f) Optical image of nanostructured hBN metalenses. (g-h) Intensity profiles of focal spots measured from hBN metalenses shown in (f). Optical imaging using hBN metalenses shown in (f). Figures are adapted with permission from: (a-c) [114], Nature Publishing Group; (d) [115], American Association for the Advancement of Science; (e) [116], Nature Publishing Group; (f-h) [117], American Chemical Society.

Nanophotonic structures integrated with vdW materials enable many novel devices, useful for photonic integrated circuits. It is expected that the vdW materials will provide more opportunities to this research field, as vdW family is still expanding and their unusual properties are revealed all the time. For instance, many TMDCs possess unique valley pseudospin properties [118]. By exploiting these features, it is possible to develop valley-optoelectronics to further expand the bandwidth of optical information processing, because the valley information can be either encoded or decoded with the spin angular momentum of photons. Unfortunately, despite progress in TMDC-based optical spin-polarized LEDs or detectors [10,119–122], their degree of circular polarizations is still limited. Towards this end, a promising strategy is to integrate those valley-optoelectronics with chiral nanophotonic devices, and some initial works have shown the possibility to control the propagation directions of different handedness of light [123]. More recent studies have confirmed the possibility of showing ferromagnetism, ferroelectricity, superconductivity, and phase transitions, even if the thickness of vdW materials are approaching to the very limit of 2D [11]. These properties can be further built into either lateral, vertical or even mixed-dimensional vdW heterostructures [124,125], enabling new architectures and operation principles of memory or tunable 2D materials integrated photonic devices.

Despite the promising future of 2D-integrated nanophotonic devices, it is notable that many of the above-mentioned demonstrations are still at the single device level, and the 2D materials are generally obtained via mechanical exfoliation method. To extend into a system level integration, one important step is to manufacture arrays of 2D-based devices at the wafer scale. At this point, the progress of growing wafer-scale graphene using chemical vapor deposition method and TMDCs via metal–organic chemical vapor deposition techniques have shown significant promise [11,126–128]. But the synthesized materials are usually polycrystalline and the inevitably formed grain boundaries would not only cause carrier scattering but also locally affect the optical and electronic properties of materials, which could reduce the quantum efficiency of 2D-based optoelectronics. Additionally, the synthesized materials generally suffer from non-uniform doping levels and anisotropic strains across the sample. As a result, it remains challenging to fabricate an array of 2D-based devices with reproducible performances and producing the films with wafer-scale homogeneity is critical to extend the 2D or vdW integrated photonics into the system level.

At a single device level, a critical technical challenge is that the Q-factor of PhCC could degrade by more than one order of magnitude and the resonance wavelength shift significantly, as the cavity experiences multiple 2D transfer processes. Moreover, the extents of both the resonance shift and Q-degradation are random and vary between transfer to transfer. In this regard, to develop more robust transfer techniques is necessary. By reducing the additional loss from the transfer process, an electrically-driven low-threshold laser at the nanoscale and attojoule-level modulators or detectors based on 2D materials could be realized. For vdW nanophotonics, most of the reported works are focused on developing passive components. But it is noteworthy that several vdW materials have anisotropic, nonlinear or structural phase-change properties, and such features could be tuned via applying an external electric field. Thus, by engineering device architectures, it is possible to realize gate-controlled active vdW nanophotonics. Furthermore, a variety of material properties can be assembled into a single device by stacking different vdW materials together to form complicated heterostructures, which offer tremendous opportunities for developing more complicated and functional nanophotonics.

## Funding

## Acknowledgments

## References

1. K. Liu, S. Sun, A. Majumdar, and V. J. Sorger, "Fundamental Scaling Laws in Nanophotonics," Sci. Rep. **6**, 37419 (2016).
2. C. Sun, M. T. Wade, Y. Lee, J. S. Orcutt, L. Alloatti, M. S. Georgas, A. S. Waterman, J. M. Shainline, R. R. Avizienis, S. Lin, B. R. Moss, R. Kumar, F. Pavanello, A. H. Atabaki, H. M. Cook, A. J. Ou, J. C. Leu, Y. H. Chen, K. Asanović, R. J. Ram, M. A. Popović, and V. M. Stojanović, "Single-chip microprocessor that communicates directly using light," Nature **528**(7583), 534–538 (2015).
3. A. H. Atabaki, S. Moazeni, F. Pavanello, H. Gevorgyan, J. Notaros, L. Alloatti, M. T. Wade, C. Sun, S. A. Kruger, H. Meng, K. Al Qubaisi, I. Wang, B. Zhang, A. Khilo, C. V. Baiocco, M. A. Popović, V. M. Stojanović, and R. J. Ram, "Integrating photonics with silicon nanoelectronics for the next generation of systems on a chip," Nature **556**(7701), 349–354 (2018).
4. D. Nikolova, S. Rumley, D. Calhoun, Q. Li, R. Hendry, P. Samadi, and K. Bergman, "Scaling silicon photonic switch fabrics for data center interconnection networks," Opt. Express **23**(2), 1159–1175 (2015).
5. Y. C. Shen, N. C. Harris, S. Skirlo, M. Prabhu, T. Baehr-Jones, M. Hochberg, X. Sun, S. J. Zhao, H. Larochelle, D. Englund, and M. Soljacic, "Deep learning with coherent nanophotonic circuits," Nat. Photonics **11**(7), 441–446 (2017).
6. N. C. Harris, G. R. Steinbrecher, M. Prabhu, Y. Lahini, J. Mower, D. Bunandar, C. C. Chen, F. N. C. Wong, T. Baehr-Jones, M. Hochberg, S. Lloyd, and D. Englund, "Quantum transport simulations in a programmable nanophotonic processor," Nat. Photonics **11**(7), 447–452 (2017).
7. J. Wang, S. Paesani, Y. Ding, R. Santagati, P. Skrzypczyk, A. Salavrakos, J. Tura, R. Augusiak, L. Mančinska, D. Bacco, D. Bonneau, J. W. Silverstone, Q. Gong, A. Acín, K. Rottwitt, L. K. Oxenløwe, J. L. O'Brien, A. Laing, and M. G. Thompson, "Multidimensional quantum entanglement with large-scale integrated optics," Science **360**(6386), 285–291 (2018).
8. J. Sun, E. Timurdogan, A. Yaacobi, E. S. Hosseini, and M. R. Watts, "Large-scale nanophotonic phased array," Nature **493**(7431), 195–199 (2013).
9. K. F. Mak and J. Shan, "Photonics and optoelectronics of 2D semiconductor transition metal dichalcogenides," Nat. Photonics **10**(4), 216–226 (2016).
10. F. N. Xia, H. Wang, D. Xiao, M. Dubey, and A. Ramasubramaniam, "Two-dimensional material nanophotonics," Nat. Photonics **8**(12), 899–907 (2014).
11. G. R. Bhimanapati, Z. Lin, V. Meunier, Y. Jung, J. Cha, S. Das, D. Xiao, Y. Son, M. S. Strano, V. R. Cooper, L. Liang, S. G. Louie, E. Ringe, W. Zhou, S. S. Kim, R. R. Naik, B. G. Sumpter, H. Terrones, F. Xia, Y. Wang, J. Zhu, D. Akinwande, N. Alem, J. A. Schuller, R. E. Schaak, M. Terrones, and J. A. Robinson, "Recent Advances in Two-Dimensional Materials beyond Graphene," ACS Nano **9**(12), 11509–11539 (2015).
12. D. L. Duong, S. J. Yun, and Y. H. Lee, "van der Waals Layered Materials: Opportunities and Challenges," ACS Nano **11**(12), 11803–11830 (2017).
13. C. Gong, L. Li, Z. Li, H. Ji, A. Stern, Y. Xia, T. Cao, W. Bao, C. Wang, Y. Wang, Z. Q. Qiu, R. J. Cava, S. G. Louie, J. Xia, and X. Zhang, "Discovery of intrinsic ferromagnetism in two-dimensional van der Waals crystals," Nature **546**(7657), 265–269 (2017).
14. B. Huang, G. Clark, E. Navarro-Moratalla, D. R. Klein, R. Cheng, K. L. Seyler, D. Zhong, E. Schmidgall, M. A. McGuire, D. H. Cobden, W. Yao, D. Xiao, P. Jarillo-Herrero, and X. Xu, "Layer-dependent ferromagnetism in a van der Waals crystal down to the monolayer limit," Nature **546**(7657), 270–273 (2017).
15. R. J. Shiue, D. K. Efetov, G. Grosso, C. Peng, K. C. Fong, and D. Englund, "Active 2D materials for on-chip nanophotonics and quantum optics," Nanophotonics **6**(6), 1329–1342 (2017).
16. V. W. Brar, M. C. Sherrott, and D. Jariwala, "Emerging photonic architectures in two-dimensional opto-electronics," Chem. Soc. Rev. **47**(17), 6824–6844 (2018).
17. G. Wang, A. Chernikov, M. M. Glazov, T. F. Heinz, X. Marie, T. Amand, and B. Urbaszek, "Colloquium: Excitons in atomically thin transition metal dichalcogenides," Rev. Mod. Phys. **90**(2), 021001 (2018).
18. S. F. Wu, S. Buckley, A. M. Jones, J. S. Ross, N. J. Ghimire, J. Q. Yan, D. G. Mandrus, W. Yao, F. Hatami, J. Vuckovic, A. Majumdar, and X. D. Xu, "Control of two-dimensional excitonic light emission via photonic crystal," 2D Materials **1**, 1 (2014).
19. X. Gan, Y. Gao, K. Fai Mak, X. Yao, R. J. Shiue, A. van der Zande, M. E. Trusheim, F. Hatami, T. F. Heinz, J. Hone, and D. Englund, "Controlling the spontaneous emission rate of monolayer $MoS_2$ in a photonic crystal nanocavity," Appl. Phys. Lett. **103**(18), 181119 (2013).
20. S. Schwarz, S. Dufferwiel, P. M. Walker, F. Withers, A. A. P. Trichet, M. Sich, F. Li, E. A. Chekhovich, D. N. Borisenko, N. N. Kolesnikov, K. S. Novoselov, M. S. Skolnick, J. M. Smith, D. N. Krizhanovskii, and A. I. Tartakovskii, "Two-dimensional metal-chalcogenide films in tunable optical microcavities," Nano Lett. **14**(12), 7003–7008 (2014).
21. J. C. Reed, A. Y. Zhu, H. Zhu, F. Yi, and E. Cubukcu, "Wavelength tunable microdisk cavity light source with a chemically enhanced MoS2 emitter," Nano Lett. **15**(3), 1967–1971 (2015).

22. T. K. Fryett, Y. Y. Chen, J. Whitehead, Z. M. Peycke, X. D. Xu, and A. Majumdar, "Encapsulated Silicon Nitride Nanobeam Cavity for Hybrid Nanophotonics," ACS Photonics **5**(6), 2176–2181 (2018).

23. S. Hammer, H. M. Mangold, A. E. Nguyen, D. Martinez-Ta, S. Naghibi Alvillar, L. Bartels, and H. J. Krenner, "Scalable and Transfer-Free Fabrication of MoS$_2$/SiO$_2$ Hybrid Nanophotonic Cavity Arrays with Quality Factors Exceeding 4000," Sci. Rep. **7**(1), 7251 (2017).

24. Y. Chen, A. Ryou, M. R. Friedfeld, T. Fryett, J. Whitehead, B. M. Cossairt, and A. Majumdar, "Deterministic Positioning of Colloidal Quantum Dots on Silicon Nitride Nanobeam Cavities," Nano Lett. **18**(10), 6404–6410 (2018).

25. C. Javerzac-Galy, A. Kumar, R. D. Schilling, N. Piro, S. Khorasani, M. Barbone, I. Goykhman, J. B. Khurgin, A. C. Ferrari, and T. J. Kippenberg, "Excitonic Emission of Monolayer Semiconductors Near-Field Coupled to High-Q Microresonators," Nano Lett. **18**(5), 3138–3146 (2018).

26. X. Z. Liu, T. Galfsky, Z. Sun, F. N. Xia, E. C. Lin, Y. H. Lee, S. Kena-Cohen, and V. M. Menon, "Strong light-matter coupling in two-dimensional atomic crystals," Nat. Photonics **9**(1), 30–34 (2015).

27. S. Dufferwiel, S. Schwarz, F. Withers, A. A. P. Trichet, F. Li, M. Sich, O. Del Pozo-Zamudio, C. Clark, A. Nalitov, D. D. Solnyshkov, G. Malpuech, K. S. Novoselov, J. M. Smith, M. S. Skolnick, D. N. Krizhanovskii, and A. I. Tartakovskii, "Exciton-polaritons in van der Waals heterostructures embedded in tunable microcavities," Nat. Commun. **6**(1), 8579 (2015).

28. D. N. Basov, M. M. Fogler, and F. J. García de Abajo, "Polaritons in van der Waals materials," Science **354**(6309), aag1992 (2016).

29. Y. Y. Jiang, X. Lin, T. Low, B. L. Zhang, and H. S. Chen, "Group-Velocity-Controlled and Gate-Tunable Directional Excitation of Polaritons in Graphene-Boron Nitride Heterostructures," Laser Photonics Rev. **12**(5), 1800049 (2018).

30. X. Lin, I. Kaminer, X. Shi, F. Gao, Z. Yang, Z. Gao, H. Buljan, J. D. Joannopoulos, M. Soljačić, H. Chen, and B. Zhang, "Splashing transients of 2D plasmons launched by swift electrons," Sci. Adv. **3**(1), e1601192 (2017).

31. S. Wu, S. Buckley, J. R. Schaibley, L. Feng, J. Yan, D. G. Mandrus, F. Hatami, W. Yao, J. Vučković, A. Majumdar, and X. Xu, "Monolayer semiconductor nanocavity lasers with ultralow thresholds," Nature **520**(7545), 69–72 (2015).

32. Y. Ye, Z. J. Wong, X. F. Lu, X. J. Ni, H. Y. Zhu, X. H. Chen, Y. Wang, and X. Zhang, "Monolayer excitonic laser," Nat. Photonics **9**(11), 733–737 (2015).

33. O. Salehzadeh, M. Djavid, N. H. Tran, I. Shih, and Z. Mi, "Optically Pumped Two-Dimensional MoS2 Lasers Operating at Room-Temperature," Nano Lett. **15**(8), 5302–5306 (2015).

34. Y. Li, J. Zhang, D. Huang, H. Sun, F. Fan, J. Feng, Z. Wang, and C. Z. Ning, "Room-temperature continuous-wave lasing from monolayer molybdenum ditelluride integrated with a silicon nanobeam cavity," Nat. Nanotechnol. **12**(10), 987–992 (2017).

35. R. Cheng, D. Li, H. Zhou, C. Wang, A. Yin, S. Jiang, Y. Liu, Y. Chen, Y. Huang, and X. Duan, "Electroluminescence and photocurrent generation from atomically sharp WSe2/MoS2 heterojunction p-n diodes," Nano Lett. **14**(10), 5590–5597 (2014).

36. J. S. Ross, P. Klement, A. M. Jones, N. J. Ghimire, J. Yan, D. G. Mandrus, T. Taniguchi, K. Watanabe, K. Kitamura, W. Yao, D. H. Cobden, and X. Xu, "Electrically tunable excitonic light-emitting diodes based on monolayer WSe2 p-n junctions," Nat. Nanotechnol. **9**(4), 268–272 (2014).

37. A. Pospischil, M. M. Furchi, and T. Mueller, "Solar-energy conversion and light emission in an atomic monolayer p-n diode," Nat. Nanotechnol. **9**(4), 257–261 (2014).

38. B. W. H. Baugher, H. O. H. Churchill, Y. Yang, and P. Jarillo-Herrero, "Optoelectronic devices based on electrically tunable p-n diodes in a monolayer dichalcogenide," Nat. Nanotechnol. **9**(4), 262–267 (2014).

39. F. Withers, O. Del Pozo-Zamudio, A. Mishchenko, A. P. Rooney, A. Gholinia, K. Watanabe, T. Taniguchi, S. J. Haigh, A. K. Geim, A. I. Tartakovskii, and K. S. Novoselov, "Light-emitting diodes by band-structure engineering in van der Waals heterostructures," Nat. Mater. **14**(3), 301–306 (2015).

40. C. H. Liu, G. Clark, T. Fryett, S. Wu, J. Zheng, F. Hatami, X. Xu, and A. Majumdar, "Nanocavity Integrated van der Waals Heterostructure Light-Emitting Tunneling Diode," Nano Lett. **17**(1), 200–205 (2017).

41. G. T. Reed, G. Mashanovich, F. Y. Gardes, and D. J. Thomson, "Silicon optical modulators," Nat. Photonics **4**(8), 518–526 (2010).

42. M. Liu, X. Yin, E. Ulin-Avila, B. Geng, T. Zentgraf, L. Ju, F. Wang, and X. Zhang, "A graphene-based broadband optical modulator," Nature **474**(7349), 64–67 (2011).

43. M. Liu, X. Yin, and X. Zhang, "Double-layer graphene optical modulator," Nano Lett. **12**(3), 1482–1485 (2012).

44. H. Dalir, Y. Xia, Y. Wang, and X. Zhang, "Athermal broadband graphene optical modulator with 35 GHz speed," ACS Photonics **3**(9), 1564–1568 (2016).

45. Y. T. Hu, M. Pantouvaki, J. Van Campenhout, S. Brems, I. Asselberghs, C. Huyghebaert, P. Absil, and D. Van Thourhout, "Broadband 10 Gb/s operation of graphene electro-absorption modulator on silicon," Laser Photonics Rev. **10**(2), 307–316 (2016).

46. A. Majumdar, J. Kim, J. Vuckovic, and F. Wang, "Electrical control of silicon photonic crystal cavity by graphene," Nano Lett. **13**(2), 515–518 (2013).

47. X. Gan, R. J. Shiue, Y. Gao, K. F. Mak, X. Yao, L. Li, A. Szep, D. Walker, Jr., J. Hone, T. F. Heinz, and D. Englund, "High-contrast electrooptic modulation of a photonic crystal nanocavity by electrical gating of graphene," Nano Lett. **13**(2), 691–696 (2013).

48. C. Qiu, W. Gao, R. Vajtai, P. M. Ajayan, J. Kono, and Q. Xu, "Efficient modulation of 1.55 μm radiation with gated graphene on a silicon microring resonator," Nano Lett. **14**(12), 6811–6815 (2014).

49. Y. Ding, X. Zhu, S. Xiao, H. Hu, L. H. Frandsen, N. A. Mortensen, and K. Yvind, "Effective electro-optical modulation with high extinction ratio by a graphene-silicon microring resonator," Nano Lett. **15**(7), 4393–4400 (2015).

50. L. A. Shiramin, W. Q. Xie, B. Snyder, P. De Heyn, P. Verheyen, G. Roelkens, and D. Van Thourhout, "High extinction ratio hybrid graphene-silicon photonic crystal switch," IEEE Photonics Technol. Lett. **30**(2), 157–160 (2018).

51. Y. Gao, R. J. Shiue, X. Gan, L. Li, C. Peng, I. Meric, L. Wang, A. Szep, D. Walker, Jr., J. Hone, and D. Englund, "High-speed electro-optic modulator integrated with graphene-boron nitride heterostructure and photonic crystal nanocavity," Nano Lett. **15**(3), 2001–2005 (2015).

52. C. T. Phare, Y. H. D. Lee, J. Cardenas, and M. Lipson, "Graphene electro-optic modulator with 30 GHz bandwidth," Nat. Photonics **9**(8), 511–514 (2015).

53. A. Vakil and N. Engheta, "Transformation optics using graphene," Science **332**(6035), 1291–1294 (2011).

54. J. Zheng, L. Yu, S. He, and D. Dai, "Tunable pattern-free graphene nanoplasmonic waveguides on trenched silicon substrate," Sci. Rep. **5**(1), 7987 (2015).

55. A. N. Grigorenko, M. Polini, and K. S. Novoselov, "Graphene plasmonics," Nat. Photonics **6**(11), 749–758 (2012).

56. D. Ansell, I. P. Radko, Z. Han, F. J. Rodriguez, S. I. Bozhevolnyi, and A. N. Grigorenko, "Hybrid graphene plasmonic waveguide modulators," Nat. Commun. **6**(1), 8846 (2015).

57. Y. Ding, X. Guan, X. Zhu, H. Hu, S. I. Bozhevolnyi, L. K. Oxenløwe, K. J. Jin, N. A. Mortensen, and S. Xiao, "Efficient electro-optic modulation in low-loss graphene-plasmonic slot waveguides," Nanoscale **9**(40), 15576–15581 (2017).

58. V. J. Sorger, R. Amin, J. B. Khurgin, Z. Z. Ma, H. Dalir, and S. Khan, "Scaling vectors of attoJoule per bit modulators," J. Opt. **20**(1), 014012 (2018).

59. S. J. Koester, H. Li, and M. Li, "Switching energy limits of waveguide-coupled graphene-on-graphene optical modulators," Opt. Express **20**(18), 20330–20341 (2012).

60. V. Sorianello, M. Midrio, G. Contestabile, I. Asselberghs, J. Van Campenhout, C. Huyghebaert, I. Goykhman, A. K. Ott, A. C. Ferrari, and M. Romagnoli, "Graphene-silicon phase modulators with gigahertz bandwidth," Nat. Photonics **12**(1), 40–44 (2018).

61. G. T. Reed, *Silicon Photonics: The State of the Art* (Wiley, 2008).

62. L. H. Yu, D. X. Dai, and S. L. He, "Graphene-based transparent flexible heat conductor for thermally tuning nanophotonic integrated devices," Appl. Phys. Lett. **105**(25), 251104 (2014).

63. J. T. Kim, K. H. Chung, and C. G. Choi, "Thermo-optic mode extinction modulator based on graphene plasmonic waveguide," Opt. Express **21**(13), 15280–15286 (2013).

64. S. Gan, C. Cheng, Y. Zhan, B. Huang, X. Gan, S. Li, S. Lin, X. Li, J. Zhao, H. Chen, and Q. Bao, "A highly efficient thermo-optic microring modulator assisted by graphene," Nanoscale **7**(47), 20249–20255 (2015).

65. D. Schall, M. Mohsin, A. A. Sagade, M. Otto, B. Chmielak, S. Suckow, A. L. Giesecke, D. Neumaier, and H. Kurz, "Infrared transparent graphene heater for silicon photonic integrated circuits," Opt. Express **24**(8), 7871–7878 (2016).

66. L. H. Yu, Y. L. Yin, Y. C. Shi, D. X. Dai, and S. L. He, "Thermally tunable silicon photonic microdisk resonator with transparent graphene nanoheaters," Optica **3**(2), 159–166 (2016).

67. S. Yan, X. Zhu, L. H. Frandsen, S. Xiao, N. A. Mortensen, J. Dong, and Y. Ding, "Slow-light-enhanced energy efficiency for graphene microheaters on silicon photonic crystal waveguides," Nat. Commun. **8**, 14411 (2017).

68. H. T. Lin, Y. Song, Y. Z. Huang, D. Kita, S. Deckoff-Jones, K. Q. Wang, L. Li, J. Y. Li, H. Y. Zheng, Z. Q. Luo, H. Z. Wang, S. Novak, A. Yadav, C. C. Huang, R. J. Shiue, D. Englund, T. Gu, D. Hewak, K. Richardson, J. Kong, and J. J. Hu, "Chalcogenide glass-on-graphene photonics," Nat. Photonics **11**(12), 798–805 (2017).

69. Z. Xu, C. Qiu, Y. Yang, Q. Zhu, X. Jiang, Y. Zhang, W. Gao, and Y. Su, "Ultra-compact tunable silicon nanobeam cavity with an energy-efficient graphene micro-heater," Opt. Express **25**(16), 19479–19486 (2017).

70. P. Dong, W. Qian, H. Liang, R. Shafiiha, D. Feng, G. Li, J. E. Cunningham, A. V. Krishnamoorthy, and M. Asghari, "Thermally tunable silicon racetrack resonators with ultralow tuning power," Opt. Express **18**(19), 20298–20304 (2010).

71. Y. B. Wang, L. Liang, Y. Y. Chen, P. Jia, L. Qin, Y. Liu, Y. Q. Ning, and L. J. Wang, "Improved performance of optical phased arrays assisted by transparent graphene nanoheaters and air trenches," RSC Advances **8**(15), 8442–8449 (2018).

72. A. Majumdar and A. Rundquist, "Cavity-enabled self-electro-optic bistability in silicon photonics," Opt. Lett. **39**(13), 3864–3867 (2014).

73. K. J. A. Ooi, P. C. Leong, L. K. Ang, and D. T. H. Tan, "All-optical control on a graphene-on-silicon waveguide modulator," Sci. Rep. **7**(1), 12748 (2017).

74. S. Yang, D. C. Liu, Z. L. Tan, K. Liu, Z. H. Zhu, and S. Q. Qin, "CMOS-compatible WS2-based all-optical modulator," ACS Photonics **5**(2), 342–346 (2018).

75. L. Yu, J. Zheng, Y. Xu, D. Dai, and S. He, "Local and nonlocal optically induced transparency effects in graphene-silicon hybrid nanophotonic integrated circuits," ACS Nano **8**(11), 11386–11393 (2014).

76. W. H. Wang, Z. Z. Yan, J. F. Zhang, J. P. Lu, H. Qin, and Z. H. Ni, "High-performance position-sensitive detector based on graphene-silicon heterojunction," Optica **5**(1), 27–31 (2018).

77. F. Xia, T. Mueller, R. Golizadeh-Mojarad, M. Freitag, Y. M. Lin, J. Tsang, V. Perebeinos, and P. Avouris, "Photocurrent imaging and efficient photon detection in a graphene transistor," Nano Lett. **9**(3), 1039–1044 (2009).

78. J. Park, Y. H. Ahn, and C. Ruiz-Vargas, "Imaging of photocurrent generation and collection in single-layer graphene," Nano Lett. **9**(5), 1742–1746 (2009).

79. C. H. Liu, N. M. Dissanayake, S. Lee, K. Lee, and Z. Zhong, "Evidence for extraction of photoexcited hot carriers from graphene," ACS Nano **6**(8), 7172–7176 (2012).

80. C. H. Liu, Y. C. Chang, S. Lee, Y. Zhang, Y. Zhang, T. B. Norris, and Z. Zhong, "Ultrafast Lateral Photo-Dember Effect in Graphene Induced by Nonequilibrium Hot Carrier Dynamics," Nano Lett. **15**(6), 4234–4239 (2015).

81. M. Freitag, T. Low, F. N. Xia, and P. Avouris, "Photoconductivity of biased graphene," Nat. Photonics **7**(1), 53–59 (2013).

82. X. Xu, N. M. Gabor, J. S. Alden, A. M. van der Zande, and P. L. McEuen, "Photo-thermoelectric effect at a graphene interface junction," Nano Lett. **10**(2), 562–566 (2010).

83. J. Yan, M. H. Kim, J. A. Elle, A. B. Sushkov, G. S. Jenkins, H. M. Milchberg, M. S. Fuhrer, and H. D. Drew, "Dual-gated bilayer graphene hot-electron bolometer," Nat. Nanotechnol. **7**(7), 472–478 (2012).

84. C. H. Liu, Y. C. Chang, T. B. Norris, and Z. Zhong, "Graphene photodetectors with ultra-broadband and high responsivity at room temperature," Nat. Nanotechnol. **9**(4), 273–278 (2014).

85. F. H. L. Koppens, T. Mueller, P. Avouris, A. C. Ferrari, M. S. Vitiello, and M. Polini, "Photodetectors based on graphene, other two-dimensional materials and hybrid systems," Nat. Nanotechnol. **9**(10), 780–793 (2014).

86. M. Buscema, J. O. Island, D. J. Groenendijk, S. I. Blanter, G. A. Steele, H. S. J. van der Zant, and A. Castellanos-Gomez, "Photocurrent generation with two-dimensional van der Waals semiconductors," Chem. Soc. Rev. **44**(11), 3691–3718 (2015).

87. M. Furchi, A. Urich, A. Pospischil, G. Lilley, K. Unterrainer, H. Detz, P. Klang, A. M. Andrews, W. Schrenk, G. Strasser, and T. Mueller, "Microcavity-integrated graphene photodetector," Nano Lett. **12**(6), 2773–2777 (2012).

88. M. Engel, M. Steiner, A. Lombardo, A. C. Ferrari, H. V. Löhneysen, P. Avouris, and R. Krupke, "Light-matter interaction in a microcavity-controlled graphene transistor," Nat. Commun. **3**(1), 906 (2012).

89. X. Gan, K. F. Mak, Y. Gao, Y. You, F. Hatami, J. Hone, T. F. Heinz, and D. Englund, "Strong enhancement of light-matter interaction in graphene coupled to a photonic crystal nanocavity," Nano Lett. **12**(11), 5626–5631 (2012).

90. R. J. Shiue, X. T. Gan, Y. D. Gao, L. Z. Li, X. W. Yao, A. Szep, D. Walker, Jr., J. Hone, and D. Englund, "Enhanced photodetection in graphene-integrated photonic crystal cavity," Appl. Phys. Lett. **103**(24), 241109 (2013).

91. X. M. Wang, Z. Z. Cheng, K. Xu, H. K. Tsang, and J. B. Xu, "High-responsivity graphene/silicon-heterostructure waveguide photodetectors," Nat. Photonics **7**(11), 888–891 (2013).

92. A. Pospischil, M. Humer, M. M. Furchi, D. Bachmann, R. Guider, T. Fromherz, and T. Mueller, "CMOS-compatible graphene photodetector covering all optical communication bands," Nat. Photonics **7**(11), 892–896 (2013).

93. X. T. Gan, R. J. Shiue, Y. D. Gao, I. Meric, T. F. Heinz, K. Shepard, J. Hone, S. Assefa, and D. Englund, "Chip-integrated ultrafast graphene photodetector with high responsivity," Nat. Photonics **7**(11), 883–887 (2013).

94. D. Schall, D. Neumaier, M. Mohsin, B. Chmielak, J. Bolten, C. Porschatis, A. Prinzen, C. Matheisen, W. Kuebart, B. Junginger, W. Templ, A. L. Giesecke, and H. Kurz, "50 GBit/s Photodetectors Based on Wafer-Scale Graphene for Integrated Silicon Photonic Communication Systems," ACS Photonics **1**(9), 781–784 (2014).

95. R. J. Shiue, Y. Gao, Y. Wang, C. Peng, A. D. Robertson, D. K. Efetov, S. Assefa, F. H. L. Koppens, J. Hone, and D. Englund, "High-Responsivity Graphene-Boron Nitride Photodetector and Autocorrelator in a Silicon Photonic Integrated Circuit," Nano Lett. **15**(11), 7288–7293 (2015).

96. S. Schuler, D. Schall, D. Neumaier, L. Dobusch, O. Bethge, B. Schwarz, M. Krall, and T. Mueller, "Controlled Generation of a p-n Junction in a Waveguide Integrated Graphene Photodetector," Nano Lett. **16**(11), 7107–7112 (2016).

97. D. Schall, C. Porschatis, M. Otto, and D. Neumaier, "Graphene photodetectors with a bandwidth >76 GHz fabricated in a 6 " wafer process line," J. Phys. D Appl. Phys. **50**(12), 124004 (2017).

98. E. P. Daniel Schall, Guillaume Ducournau, Vanessa Avramovic, Martin Otto, Daniel Neumaier, "Record high bandwidth integrated graphene photodetectors for communication beyond 180 Gb/s," arXiv:1804.10016.

99. N. Youngblood, C. Chen, S. J. Koester, and M. Li, "Waveguide-integrated black phosphorus photodetector with high responsivity and low dark current," Nat. Photonics **9**(4), 247–252 (2015).

100. D. Jariwala, A. R. Davoyan, G. Tagliabue, M. C. Sherrott, J. Wong, and H. A. Atwater, "Near-Unity Absorption in van der Waals Semiconductors for Ultrathin Optoelectronics," Nano Lett. **16**(9), 5482–5487 (2016).

101. D. Jariwala, A. R. Davoyan, J. Wong, and H. A. Atwater, "Van der Waals Materials for Atomically-Thin Photovoltaics: Promise and Outlook," ACS Photonics **4**(12), 2962–2970 (2017).

102. W. Y. Wang, A. Klots, Y. M. Yang, W. Li, D. P. Kravchenko II, D. P. Briggs, K. I. Bolotin, and J. Valentine, "Enhanced absorption in two-dimensional materials via Fano-resonant photonic crystals," Appl. Phys. Lett. **106**(18), 181104 (2015).

103. W. Wang, A. Klots, D. Prasai, Y. Yang, K. I. Bolotin, and J. Valentine, "Hot Electron-Based Near-Infrared Photodetection Using Bilayer MoS2," Nano Lett. **15**(11), 7440–7444 (2015).

104. L. Huang, G. Li, A. Gurarslan, Y. Yu, R. Kirste, W. Guo, J. Zhao, R. Collazo, Z. Sitar, G. N. Parsons, M. Kudenov, and L. Cao, "Atomically Thin MoS2 Narrowband and Broadband Light Superabsorbers," ACS Nano **10**(8), 7493–7499 (2016).

105. J. Wong, D. Jariwala, G. Tagliabue, K. Tat, A. R. Davoyan, M. C. Sherrott, and H. A. Atwater, "High Photovoltaic Quantum Efficiency in Ultrathin van der Waals Heterostructures," ACS Nano **11**(7), 7230–7240 (2017).

106. G. Wang, X. Marie, I. Gerber, T. Amand, D. Lagarde, L. Bouet, M. Vidal, A. Balocchi, and B. Urbaszek, "Giant enhancement of the optical second-harmonic emission of WSe$_2$ monolayers by laser excitation at exciton resonances," Phys. Rev. Lett. **114**(9), 097403 (2015).

107. T. Fryett, A. Zhan, and A. Majumdar, "Cavity nonlinear optics with layered materials," Nanophotonics **7**(2), 355–370 (2018).

108. A. Majumdar, C. M. Dodson, T. K. Fryett, A. Zhan, S. Buckley, and D. Gerace, "Hybrid 2D Material Nanophotonics: A Scalable Platform for Low-Power Nonlinear and Quantum Optics," ACS Photonics **2**(8), 1160–1166 (2015).

109. J. K. Day, M. H. Chung, Y. H. Lee, and V. M. Menon, "Microcavity enhanced second harmonic generation in 2D MoS2," Opt. Mater. Express **6** (7), 2360–2365 (2016).

110. T. K. Fryett, K. L. Seyler, J. J. Zheng, C. H. Liu, X. D. Xu, and A. Majumdar, "Silicon photonic crystal cavity enhanced second-harmonic generation from monolayer WSe2," 2D Materials **4**, 1 (2017).

111. H. Chen, V. Corboliou, A. S. Solntsev, D. Y. Choi, M. A. Vincenti, D. de Ceglia, C. de Angelis, Y. Lu, and D. N. Neshev, "Enhanced second-harmonic generation from two-dimensional MoSe$_2$ on a silicon waveguide," Light Sci. Appl. **6**(10), e17060 (2017).

112. F. Yi, M. Ren, J. C. Reed, H. Zhu, J. Hou, C. H. Naylor, A. T. C. Johnson, R. Agarwal, and E. Cubukcu, "Optomechanical Enhancement of Doubly Resonant 2D Optical Nonlinearity," Nano Lett. **16**(3), 1631–1636 (2016).

113. T. K. Fryett, A. Zhan, and A. Majumdar, "Phase-matched nonlinear optics via patterning layered materials," Opt. Lett. **42**(18), 3586–3589 (2017).

114. J. Yang, Z. Wang, F. Wang, R. Xu, J. Tao, S. Zhang, Q. Qin, B. Luther-Davies, C. Jagadish, Z. Yu, and Y. Lu, "Atomically thin optical lenses and gratings," Light Sci. Appl. **5**(3), e16046 (2016).

115. P. Li, I. Dolado, F. J. Alfaro-Mozaz, F. Casanova, L. E. Hueso, S. Liu, J. H. Edgar, A. Y. Nikitin, S. Vélez, and R. Hillenbrand, "Infrared hyperbolic metasurface based on nanostructured van der Waals materials," Science **359**(6378), 892–896 (2018).

116. S. Kim, J. E. Fröch, J. Christian, M. Straw, J. Bishop, D. Totonjian, K. Watanabe, T. Taniguchi, M. Toth, and I. Aharonovich, "Photonic crystal cavities from hexagonal boron nitride," Nat. Commun. **9**(1), 2623 (2018).

117. C.-H. Liu, J. Zheng, S. Colburn, T. K. Fryett, A. Majumdar, S. Colburn, T. K. Fryett, Y. Chen, and X. Xu, "Ultrathin van der Waals metalenses," Nano Lett. **18**(11), 6961–6966 (2018).

118. X. D. Xu, W. Yao, D. Xiao, and T. F. Heinz, "Spin and pseudospins in layered transition metal dichalcogenides," Nat. Phys. **10**(5), 343–350 (2014).

119. Y. J. Zhang, T. Oka, R. Suzuki, J. T. Ye, and Y. Iwasa, "Electrically switchable chiral light-emitting transistor," Science **344**(6185), 725–728 (2014).

120. K. F. Mak, K. L. McGill, J. Park, and P. L. McEuen, "Valleytronics. The valley Hall effect in MoS transistors," Science **344**(6191), 1489–1492 (2014).

121. O. L. Sanchez, D. Ovchinnikov, S. Misra, A. Allain, and A. Kis, "Valley Polarization by Spin Injection in a Light-Emitting van der Waals Heterojunction," Nano Lett. **16**(9), 5792–5797 (2016).

122. Y. Ye, J. Xiao, H. Wang, Z. Ye, H. Zhu, M. Zhao, Y. Wang, J. Zhao, X. Yin, and X. Zhang, "Electrical generation and control of the valley carriers in a monolayer transition metal dichalcogenide," Nat. Nanotechnol. **11**(7), 598–602 (2016).

123. S. H. Gong, F. Alpeggiani, B. Sciacca, E. C. Garnett, and L. Kuipers, "Nanoscale chiral valley-photon interface through optical spin-orbit coupling," Science **359**(6374), 443–447 (2018).

124. D. Jariwala, T. J. Marks, and M. C. Hersam, "Mixed-dimensional van der Waals heterostructures," Nat. Mater. **16**(2), 170–181 (2017).

125. Y. Liu, N. O. Weiss, X. D. Duan, H. C. Cheng, Y. Huang, and X. F. Duan, "Van der Waals heterostructures and devices," Nat. Rev. Mater. **1**(9), 16042 (2016).

126. X. Li, W. Cai, J. An, S. Kim, J. Nah, D. Yang, R. Piner, A. Velamakanni, I. Jung, E. Tutuc, S. K. Banerjee, L. Colombo, and R. S. Ruoff, "Large-area synthesis of high-quality and uniform graphene films on copper foils," Science **324**(5932), 1312–1314 (2009).

127. S. Lee, K. Lee, C. H. Liu, and Z. Zhong, "Homogeneous bilayer graphene film based flexible transparent conductor," Nanoscale **4**(2), 639–644 (2012).

128. K. Kang, S. Xie, L. Huang, Y. Han, P. Y. Huang, K. F. Mak, C. J. Kim, D. Muller, and J. Park, "High-mobility three-atom-thick semiconducting films with wafer-scale homogeneity," Nature **520**(7549), 656–660 (2015).